



## ORIGINAL ARTICLE

# Direct sunlight photodegradation of congo red in aqueous solution by TiO<sub>2</sub>/rGO binary system: Experimental and DFT study



Mohammed Asaad Mahdi <sup>a</sup>, Mohammed A. Farhan <sup>a</sup>, Zaid H. Mahmoud <sup>a,\*</sup>,  
Ahmed Mahdi Rheima <sup>b</sup>, Zainab sabri Abbas <sup>c</sup>, Mustafa M. Kadhim <sup>d</sup>,  
Alaa dhari jawad al-bayati <sup>e</sup>, Asala Salam Jaber <sup>f</sup>, Safa K. Hachim <sup>g,h</sup>, Ahmad  
Hussain Ismail <sup>b</sup>

<sup>a</sup> Chemistry Department, College of Science, University of Diyala, Iraq

<sup>b</sup> Department of Chemistry, College of Science, Mustansiriyah University, Baghdad, Iraq

<sup>c</sup> Wasit University, College of Science, Department of Chemistry, Iraq

<sup>d</sup> Medical Laboratory Techniques Department, Al-Farahidi University, Baghdad 10022, Iraq

<sup>e</sup> Department of Chemical Engineering and Petroleum Industries, Al-Mustaqbal University College, 51001 Hilla, Iraq

<sup>f</sup> Department of Pharmacy, Mazaya University College, Thi-Qar, Iraq

<sup>g</sup> College of Technical Engineering, The Islamic University, Najaf, Iraq

<sup>h</sup> Department of Medical Laboratory, College of Health and Medical Technology, National University of Science and Technology, Thi-Qar 64001, Iraq

Received 4 February 2023; accepted 9 May 2023

Available online 15 May 2023

## KEYWORDS

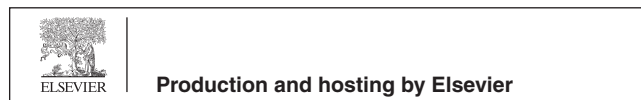
Mass;  
DFT;  
Theoretical;  
XPS

**Abstract** Photolysis was employed to produce titanium dioxide (TiO<sub>2</sub>) with exposed (001) facets, which were then modified by incorporating reduce graphene oxide (rGO) sheets at (1, 3 and 5) wt. %. The chemical composition, optical properties, morphology, and electrochemical behavior of both the pure and composite nanomaterials were analyzed. The X-ray diffraction (XRD) and Raman spectroscopy techniques confirmed the formation of the anatase phase of TiO<sub>2</sub> in the samples. The Debye Scherrer method was utilized to estimate the size of the particles. It was observed that the particle size decreased as the concentration of rGO increased; at 5 wt% rGO, the size was 11 nm. The morphology of the rGO/TiO<sub>2</sub> nanocomposite was analyzed with transmission electron microscopy (TEM) which showed that TiO<sub>2</sub> nanoparticles were dispersed on the surface of the rGO

\* Corresponding author.

E-mail address: [zaidhameed\\_91@yahoo.com](mailto:zaidhameed_91@yahoo.com) (Z.H. Mahmoud).

Peer review under responsibility of King Saud University.



sheets. The analysis of the X-ray photoelectron spectrum (XPS) revealed that bonding of TiO<sub>2</sub> with rGO occurred through the formation of Ti-C and Ti-O-C bonds. The results obtained from the diffuse reflectance spectroscopy (DRS) showed a decrease in band gap upon an increase in rGO concentration. Moreover, confirmation was obtained regarding the reduction of recombination carriers through the photoluminescence (PL) spectrum. The results indicated that the prepared nanocomposite had a high number of oxygen vacancies. The photodegradation mechanism of congo red dye under sunlight was studied by Liquid chromatography–mass spectrometry (LC-Mass) and scavenger effect. The photodegradation of congo red dye (CR) utilizing TiO<sub>2</sub>, both pure and incorporated with rGO, was observed under normal conditions in the presence of sunlight. The study revealed that the optimal condition for achieving maximum photodegradation of CR dye was pH = 7, 100 min, 50 ppm initial CR dye concentration and 10 mg of catalyst dosage. The photodegradation data illustrated that 5 wt% rGO doped TiO<sub>2</sub> exhibits higher efficiency than other 3; 1 wt% rGO and pure TiO<sub>2</sub>. Finally, the improving breakdown of CR dye using direct sunlight showed high efficiency without leaving behind any secondary intermediates.

© 2023 The Author(s). Published by Elsevier B.V. on behalf of King Saud University. This is an open access article under the CC BY-NC-ND license (<http://creativecommons.org/licenses/by-nc-nd/4.0/>).

## 1. Introduction

In recent years, there has been a significant focus on advocating for clean energy sources due to the increasing challenges related to energy and the environment (Mahmoud et al., 2018; Farhan et al., 2018). Solar energy has the potential to foster environmentally conscious communities. In this regard, significant research efforts are dedicated towards converting solar energy into usable energy (Mahmoud et al., 2022). This energy is presently utilized in applications such as photochemical cells, solar cells, and photocatalysis (Mahmoud et al., 2022). The photocatalytic degradation of organic dye pollutants has generated substantial interest due to its practical applications and economic benefits. Various types of nanoparticles have been developed and synthesized with the objective of enhancing the natural environment. The semiconductor materials have garnered attention from various other materials because of non-toxicity, no secondary pollution, stable chemical and low cost (Moushumi et al., 2022; Kundu and Mondal, 2019; Saher et al., 2021). Amongst different semiconductor materials, the anatase phase of TiO<sub>2</sub> is considered to have the greatest potential for practical applications (Aoudjit et al., 2021). Moreover, the TiO<sub>2</sub> nanoparticles possess a significantly large surface area, rendering them highly effective in enhancing sunlight adsorption as compared to bulk particles (Reza et al., 2017). There exist two big significant challenges for this material. Firstly, its band gap has a relatively large value of (3–3.2) eV, limiting its response to UV light only. Secondly, the material experiences a high rate of recombination for electron-hole pairs (Saeed et al., 2017). Various techniques have been employed to restore the photocatalytic activity of photocatalysts in order to overcome these issues, however, satisfactory outcomes have not been achieved thus far. Graphene, a novel type of carbon material featuring a two-dimensional sp<sup>2</sup> network, has generated considerable interest due to its unique structure, remarkable thermal and chemical stability, and exceptional conductivity (Fathy et al., 2016). Graphene is considered to be an optimal support for photocatalysts due to its ability to enhance the activity of photocatalysis by facilitating the transfer of electrons from the conduction band (CB) of anatase, thereby prolonging the lifespan of h-e pairs (Du et al., 2022). Numerous studies have demonstrated that

the incorporation of graphene oxide (GO) into TiO<sub>2</sub>/rGO nanocomposites can enhance electron transfer and reduce the rate of e-h recombination (Ma et al., 2021). Long et al., (Long and Qin, 2013) reported the activity of 0.8 wt% rGO doped TiO<sub>2</sub> in photodegradation of dye under sunlight, allocating the activity to the p-n junction heterostructure formed between TiO<sub>2</sub> and rGO. Andreozzi et al., (Andreozzi et al., 2018) reported that the purification of water contains high ratio of saline and different organic dye and organic compounds using 10 wt% rGO-TiO<sub>2</sub>. The increase in photocatalytic performance can be attributed to the favorable charge transfer characteristics of rGO. It also exhibits high load mobility and rapid transfer of charges during its structure, which can be advantageous in redox reactions (Fang et al., 2015; Mahmoud et al., 2023). The properties of a composite material are not merely a combination of the properties of its individual components. Rather, the surface reactions and interactions between semiconductors contribute significantly to its unique properties (Al-Obaidi et al., 2023). The production of rGO-TiO<sub>2</sub> heterostructures enables the absorption of a wide range of wavelengths and subsequent separation of electron-hole pairs, resulting in an increase in photocatalytic activity (Mahmoud et al., 2021). The objective of this investigation is to identify the specific reactive oxygen species (ROS) responsible for the photodegradation process of %wt. rGO doped TiO<sub>2</sub> nanostructure, in order to gain a better understanding of the photodegradation mechanism for congo red organic dye and the factors that influence the activity of these heterostructures. A method for rapid synthesis of TiO<sub>2</sub>-incorporated rGO using photolysis-assisted hydrothermal treatment, resulting in improved photocatalytic activity, was proposed. The anatase TiO<sub>2</sub> phase was characterized via XRD and TEM, and rGO was confirmed via Raman spectrum. TEM confirms the interaction between TiO<sub>2</sub> agglomeration nanoparticles and rGO nano sheets. The samples of %wt. rGO-TiO<sub>2</sub> exhibit a distinct spectral behavior as observed through DRS. PL results were studied to investigate the separation and transportation of photo-carriers. Finally, the photocatalytic mechanism modulation of %wt. rGO-TiO<sub>2</sub> compared with TiO<sub>2</sub> in congo red dye photodegradation was proved during scavenger solutions. The introduction of rGO altered the intermediate reactive oxygen, leading to an increase in activity under sunlight illumination. This confirms that the

use of rGO leads to changes that enhance the photocatalytic activity of TiO<sub>2</sub>.

## 2. Experimental

### 2.1. Materials

All chemicals materials (graphite powder (99.9%), sodium nitrate (98%), hydrogen peroxide (30%), potassium permanganate (98%), sodium hydroxide (97%), hydrochloric acid (36%), ethanol (70%), titanium isopropoxide (99%) and congo red dye (C<sub>32</sub>H<sub>24</sub>N<sub>6</sub>O<sub>6</sub>S<sub>2</sub>.2Na, λ<sub>max</sub> = 497 nm)) were supplied from sigma Aldrich company and used without any future purification. All solution prepared by using distilled water.

### 2.2. Preparation of titanium oxide (TiO<sub>2</sub>)

The synthesis of TiO<sub>2</sub> was reported by Zaid et al., 2020 (Mahmoud et al., 2022). 10 ml of isopropoxide stock solution was diluted by 40 ml distilled water and irradiated using manual irradiation 15 W power system in ice bath (Fig. S1, supplementary information). The irradiation process was carried out until a white precipitate was obtained, which was subsequently separated from the solution through decantation and washed by acetone, ethanol and distilled water. Finally, it dried at 80 °C for 5 h and calcined at 500 °C for 2 h.

### 2.3. Preparation of graphene oxide (GO)

The preparation of GO was carried out by using Hemmer modified method (Khatmi Maab et al., 2016). Firstly, in 300 ml beaker, (1gm, 2gm and 36 ml) of graphite powder, sodium nitrate and 1 M H<sub>2</sub>SO<sub>4</sub> were mixed together in ice bath for 4 h. then, 5gm of potassium permanganate was added to mixture slowly under strong stirring. Next, 200 ml of warm water was added to the mixture. While continuously stirring, 35 ml of 30% hydrogen peroxide was gradually added until the color changed to yellow. Finally, the suspension solution of graphene isolated by decantation and washed several times by distilled water and 10% HCl before dried at 60 °C for 3 h.

### 2.4. Preparation of graphene oxide/Titanium oxide (rGO/TiO<sub>2</sub>)nanocomposite

The preparation of rGO/TiO<sub>2</sub> nanocomposite was carried out using hydrothermal method. Firstly, various weight ratios of rGO (1%, 3%, and 5%) were mixed with an equivalent amount of TiO<sub>2</sub> solution and sonicated for 45 min until a brown solution was obtained. Next, the rGO/TiO<sub>2</sub> suspension was transferred to stainless steel auto-cleave and heated to 200 °C for 6 h and allowed to cool down naturally at room temperature. Finally, the gray precipitate of rGO/TiO<sub>2</sub> was transferred and isolated by centrifuging process before washing it several times by ethanol and distilled water (Shen et al., 2011; Yue et al., 2019; Liu et al., 2016).

### 2.5. Study of photocatalytic activity

The photocatalytic activity of (1, 3 and 5%) of rGO/TiO<sub>2</sub> were investigated for degradation of CR dye solution. The solution

reaction was prepared by adding 0.01gm of each prepared materials in 100 ml of 10 ppm dye solution. Firstly, the resulting suspension was then stirred in a dark environment for 30 min to achieve adsorption–desorption equilibrium. The subsequent step involved exposing the sample to direct sunlight for varying durations using a manual irradiation system with an intensity of 1200 W.cm<sup>-2</sup> (Fig. S2, supplementary information). To maintain a constant temperature during the reaction, the water was circulated around the reactor. At pre-determined intervals, a 5 ml sample of the solution was collected and subjected to centrifugation to remove the catalyst. The remaining concentration was then analyzed using UV–Vis spectrum and LC-MS techniques.

## 3. Results and discussion

### 3.1. Structural characterization

The XRD of TiO<sub>2</sub> and (1, 3 and 5) wt.% rGO/TiO<sub>2</sub> are shown in Fig. 1a-d. The observed patterns exhibit peaks that can be attributed to the formation of TiO<sub>2</sub> with lattice parameter of a = b = 3.78 and c = 9.50 and the results are in agreement with JCPDS (04-0477). The diffraction pattern of pure TiO<sub>2</sub> (Fig. 3a) displayed peaks at angles of 25.35°, 37.78°, 48.07°, 53.93°, 55.11° and 62.72° corresponding to (101), (004), (200), (105), (211) and (204) respectively, indicating the presence of a tetragonal anatase phase. In Fig. 1b-d, it can be observed that the anatase phase remains unchanged for all diffraction peaks, irrespective of the rGO mass ratio dopant. This observation indicates that the prepared TiO<sub>2</sub> is stabilized. The XRD patterns illustrated in Fig. 1b and 1c for TiO<sub>2</sub> doped with 1% and 3% GO respectively do not exhibit any peaks that can be attributed to rGO. This may be due to the high degree of isolation of rGO sheets by TiO<sub>2</sub> nanoparticles (Moustafa et al., 2022). However, the diffraction peak centered at 10.99°, which corresponds to (001), is observed and can be attributed to rGO. rGO/TiO<sub>2</sub> was estimated by using Scherrer equation (Holzwarth and Gibson, 2011):

$$D = \frac{0.9\lambda}{\beta \cos\theta} \quad (1)$$

Where 0.9: is shape factor, λ: X-ray source wavelength, β: full width at half maximum of peak. Table 1 presents the findings that reveal a decrease in crystallite size as the dopant weight ratio increases. This is indicative of rGO segregation at the TiO<sub>2</sub> boundaries, thereby inhibiting crystal growth. On the other side, slight elongation of c axis is shown (Table. 1), while a and b axis remain constant, that the carbon of GO fcc and bcc is positioned at the center or occupied in the structure of TiO<sub>2</sub> (Ma et al., 2021).

Raman spectrum technique was used to investigate the chemical composition and the structure of prepared compounds through vibrational properties. The spectrum of GO, rGO and rGO/TiO<sub>2</sub> are shown in Fig. 2a-c, respectively. At Fig. 2a, two bands can be observed that are centered at 1350 cm<sup>-1</sup>(D) and 1595 cm<sup>-1</sup> (G) assigned to sp<sup>3</sup> defect and sp<sup>2</sup> in plane vibration carbon atoms. Additionally, at the Brillouin zone, the E<sub>2g</sub> doubly degenerated mode can be observed (Krishnamoorthy et al., 2012). The spectrum of rGO (Fig. 2b) illustrates a shift in the G band towards lower wavelengths (1595 to 1584 cm<sup>-1</sup>) while the D band remains unshifted. This

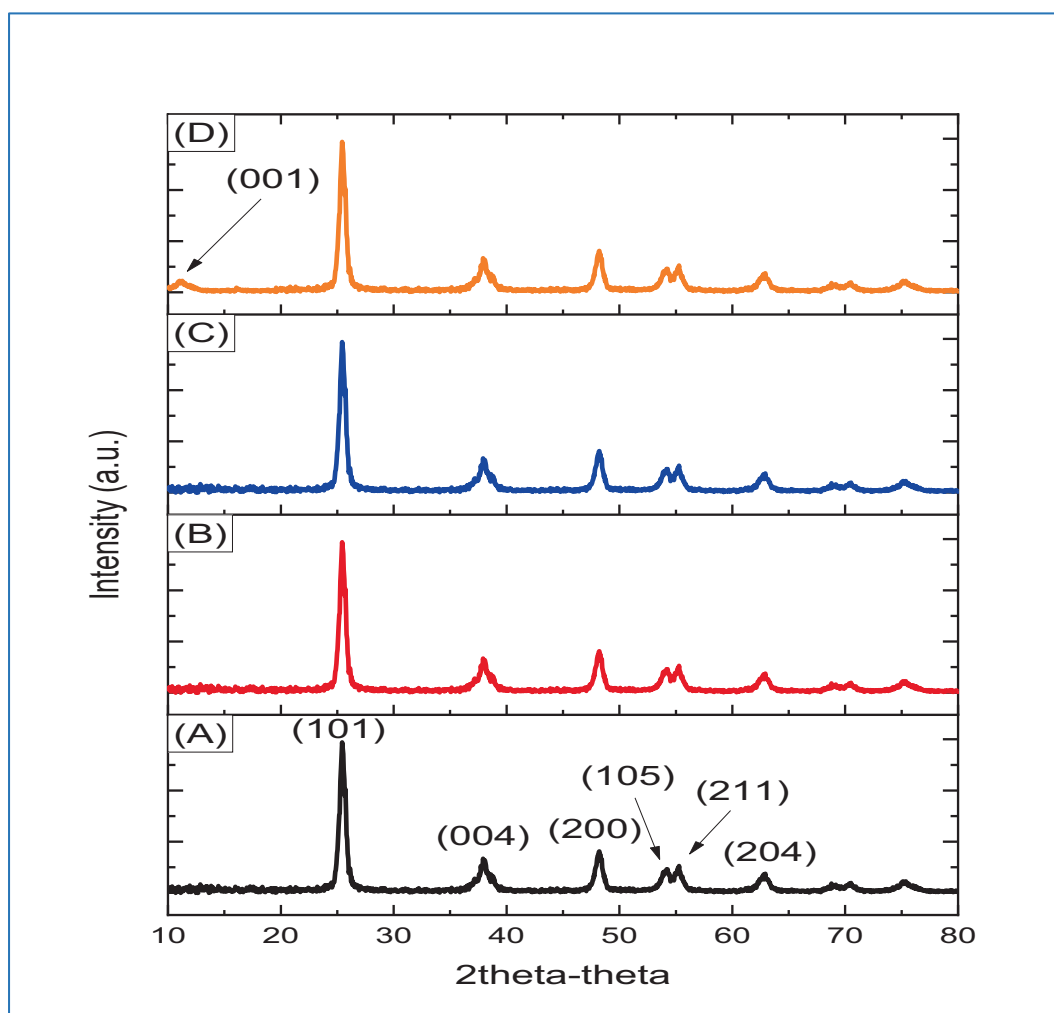


Fig. 1 XRD of pure and 1,3 and 5 wt% rGO doping TiO<sub>2</sub>.

**Table 1** Size particles of tio<sub>2</sub> and %wt. rGO-TiO<sub>2</sub>.

photocatalyst	2θ of (101) crystal plane	Lattice parameter (Å)		FWHM	D (nm)
		a = b	c		
TiO <sub>2</sub>	25.46	3.78	9.532	0.67036	13
1 wt% rGO	25.30	3.78	9.541	0.72453	12
3 wt% rGO	25.18	3.78	9.552	0.78493	11
5 wt% rGO	25.12	3.78	9.5605	0.80546	10

may be attributed to the self-healing properties of rGO, whereby carbon atoms are restored to the hexagonal network (Chen et al., 2021). This downshift in G band indicate the successful reduction to rGO. In Fig. 2c, the two bands of D and G exhibit broadening in the rGO/TiO<sub>2</sub> nanocomposite, which can be attributed to the stacking of rGO sheets induced by carbonyl groups attached to rGO. This leads to a hindrance in the accumulation of rGO sheets. The disorder structure of prepared compounds are measured based on the ID/IG ratio. The findings indicate that the ratio experienced an increase from 0.9 to 0.98 as a consequence of the reduction of GO to rGO. This outcome can be attributed to the defects and elim-

ination of functional groups (carboxylic acid) present on the surface of GO (Ansari et al., 2022). On the other hand, slight reduce in the ratio value (0.85) is shown in rGO/TiO<sub>2</sub> nanocomposite due to the reduction of sp<sup>3</sup> to sp<sup>2</sup> carbon atoms as well as, reducing in the domain size of sp<sup>2</sup> during hydrothermal process (Karthik et al., 2020). Fig. 4d illustrates the zoomed spectrum of pure and (1, 3 and 5)wt.% rGO/TiO<sub>2</sub> nanocomposite with range of 100–200 cm<sup>-1</sup>. The results showed that the intensity of Eg band mode is increased with increasing the doped ratio. Additionally, this mode is shifted toward a lower wavenumber with broadening, which can be attributed to the impact of phonon confinement and surface

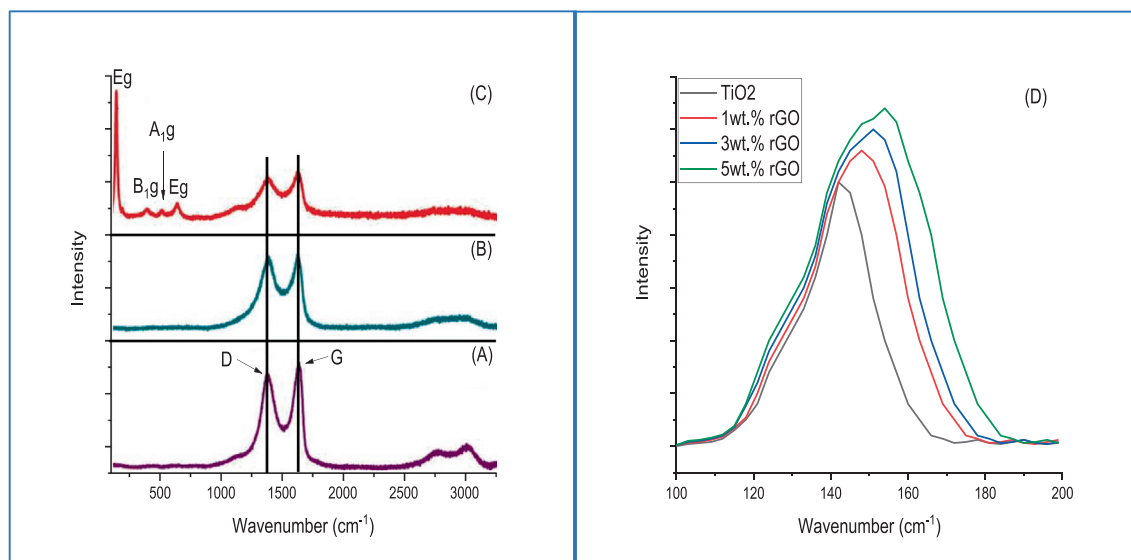


**Fig. 2** Raman spectrum of (A) GO, (B) rGO, rGO doped TiO<sub>2</sub> and (D) Eg intensity peak of TiO<sub>2</sub>.

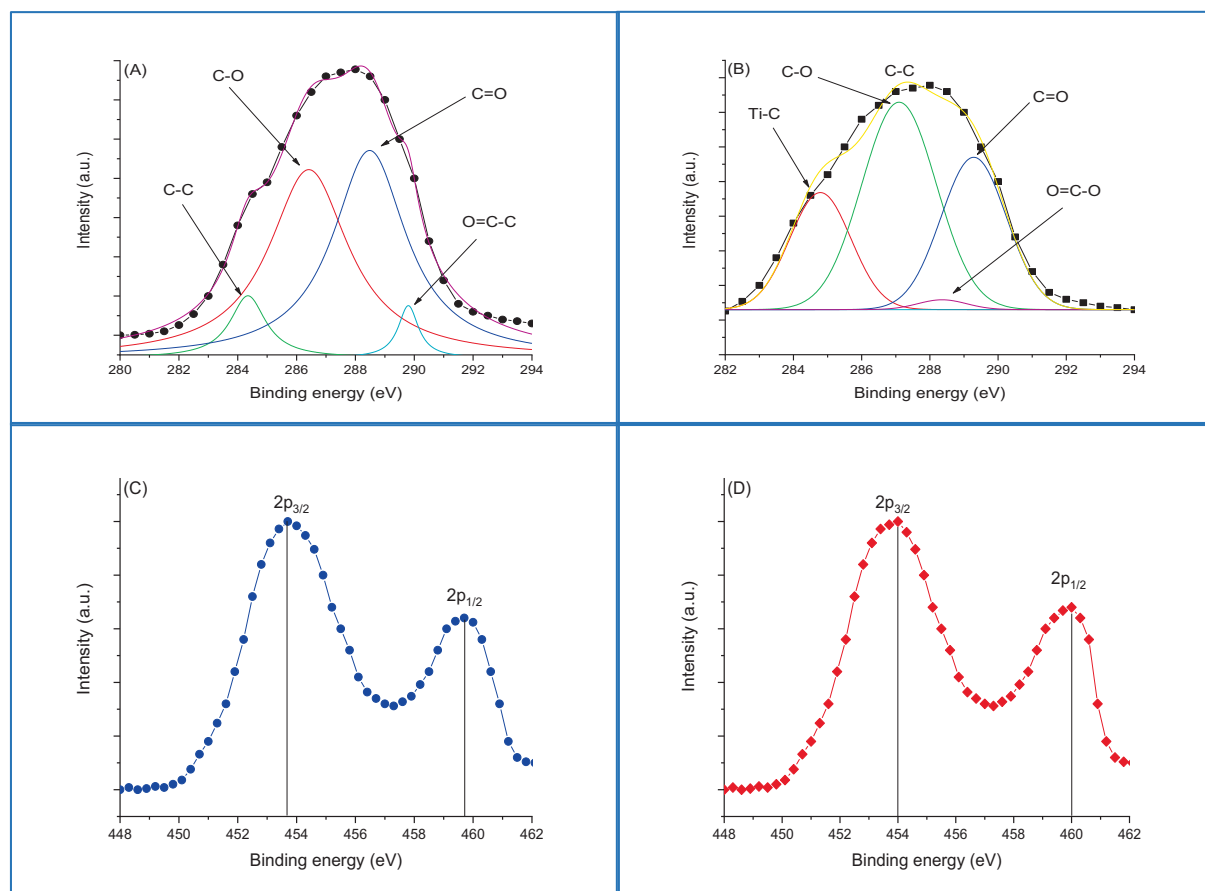


**Fig. 3** XPS of (A) C 1s, (C) 2p of rGO before doping and (B) C 1s, (D) 2p of rGO after doping.

pressure. Numerous studies (Singh et al., 2022) have addressed the shift in Raman peak position, which is attributed to two possible factors. The first posits that the intensity of TiO<sub>2</sub> peaks is affected by vacancy defects, which are amplified by the disordered structure of graphene. The second possibility

is that the shift results from electronic transitions occurring between graphene sheets and TiO<sub>2</sub>.

The chemical analysis of GO and rGO/TiO<sub>2</sub> nanocomposite was investigated by using X-ray Photoelectron Microscopy (XPS). The findings of the analysis are presented in



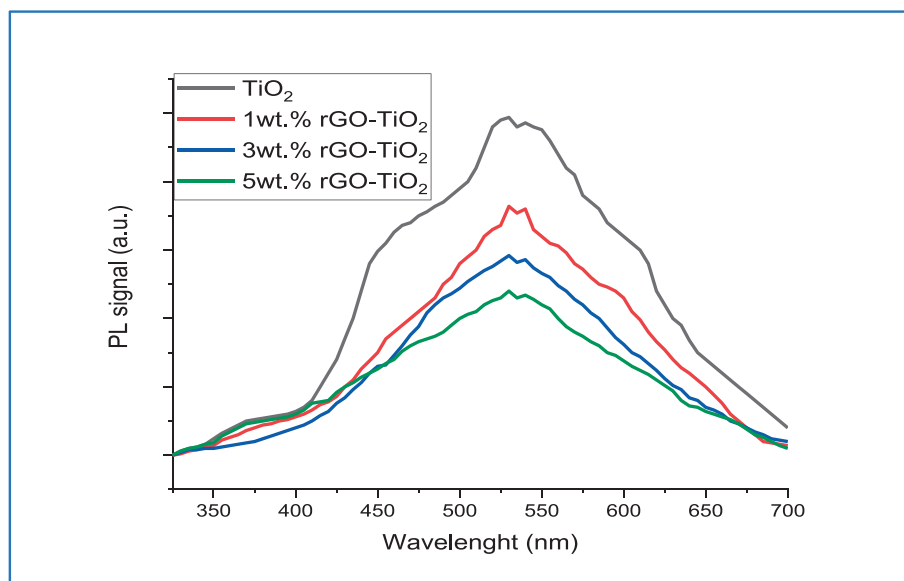


**Fig. 4** PL of pure and 1,3 and 5 wt% rGO/TiO<sub>2</sub>.

Fig. 3a-d. Fig. 6a and 6b display multiple peaks centered at binding energies of 284.6, 286.3, 287.3, and 288.9 eV, corresponding to the core level spectra of carbon and indicating the presence of carbon-carbon and carbon-oxygen bonds (Wang et al., 2020). The findings demonstrate a reduction in the intensity peaks of carbon-oxygen in rGO/TiO<sub>2</sub> nanocomposite, indicating the reduction of GO via hydrothermal processing. Additionally, a peak is observed at 282.4 eV corresponding to the Titanium-carbon bond. The core level of Ti<sup>4+</sup> in pure TiO<sub>2</sub> and rGO/TiO<sub>2</sub> nanocomposite were shown in Fig. 3c,d. Fig. 3c exhibits the presence of two intensity peaks at 453.8 and 459.1 eV, which are attributed to Ti 2p<sub>3/2</sub> and Ti 2p<sub>1/2</sub>, respectively. The difference in binding energy between these two peaks is measured to be 6.01 eV, aligning with previous findings in literature (Wang et al., 2020). The difference in binding energy of Ti<sup>4+</sup> remains present in rGO/TiO<sub>2</sub> nanocomposite as shown in Fig. 3d, but the binding energies of Ti 2p<sub>3/2</sub> and Ti 2p<sub>1/2</sub> increased because of the interaction between titanium and carbonyl groups of rGO (Dong et al., 2017).

The crystal lattice of TiO<sub>2</sub> was analyzed to examine the defect and vacancy of oxygen ions using PL spectrum. The results are depicted in Fig. 4, which displays a wide peak containing four sub-band emissions positioned at 420, 487, 520, and 680 nm correspondingly. The emission band at 420 nm assigned to the interaction of h<sup>+</sup> - e<sup>-</sup> or may be attributed to self-trapped exciton (Dong et al., 2017). A sub-band at 487 nm is observed and attributed to the transfer of electrons from Ti<sup>3+</sup> to O<sup>2-</sup> in octahedral complex (Dong et al., 2017). Additionally, two sub-bands located at 520 and 680 nm are linked to self-trapped oxygen vacancies known as F centers (Nasralla et al., 2020). The PL spectrums of (1, 3 and 5)wt. % rGO incorporated TiO<sub>2</sub> are demonstrated at Fig. 4.b-d. The results demonstrate that as the concentration of rGO increases, there is a gradual reduction in the intensity of emission peaks. This phenomenon is attributed to peak quenching via rGO incorporation, and becomes more apparent at 5 wt% rGO sheet doping. The reduction in intensity is contingent

upon the interplay of ions. At a 1 wt% incorporation ratio, the interaction between ions is insufficient to significantly impact energy levels. Conversely, with a 5 wt% incorporation ratio, the interaction between ions is considerably stronger due to a decrease in defects and an increase in ion concentration (Chetibi et al., 2017), ultimately resulting in quenching (John et al., 2020). There are two factors that contribute to the quenching of emission peaks. The first factor is non-radiative energy loss, which arises from the transfer of energy from ions to defect sites. The second factor involves the scattering of electrons by oxygen ions at states of trapping, which results in an increase in the duration of h<sup>+</sup>-e<sup>-</sup> recombination (Sang et al., 2019).

Fig. 5 shows the band gap of pure TiO<sub>2</sub> and (1, 3 and 5)wt. % GO incorporated TiO<sub>2</sub> calculated by using Tauc plot (Chen et al., 2017). The findings indicate that there was a slight decrease in energies as the Rgo ratio increased. This could be attributed to the influence of dielectric confinement (Al-Kandari et al., 2021). This confinement is a significant factor in energy alteration and its influence surpasses that of electron-hole space confinement, leading to the observed decrease in energy levels.

TEM images were utilized to investigate the morphology of both prepared TiO<sub>2</sub> and rGO/TiO<sub>2</sub> nanocomposite. The results, as depicted in Fig. 6, reveal a uniform distribution of TiO<sub>2</sub> nanospheres on rGO sheets, with an interlayer distance in the low nanometer range. These findings are consistent with the (101) crystal plane of anatase, indicating good agreement.

### 3.2. UV-Vis and TOC

The photodegradation of congo red (CR) dye over pure TiO<sub>2</sub> and 5 wt% rGO/TiO<sub>2</sub> was studied by analyzing band gap, EIS, UV-Vis spectrum, and total organic carbon (TOC) results. The UV-Vis spectrum of CR photodegraded under sunlight over 5 wt% rGO/TiO<sub>2</sub> is depicted in Fig. 7a. The UV-Vis spectrum of CR shows strong adsorption band with range of 330-

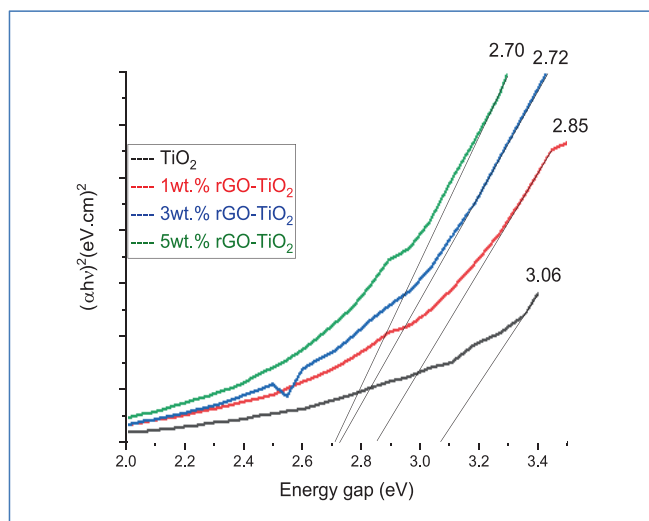


Fig. 5 Band gap of pure and 1,3 and 5 wt% rGO/TiO<sub>2</sub>.

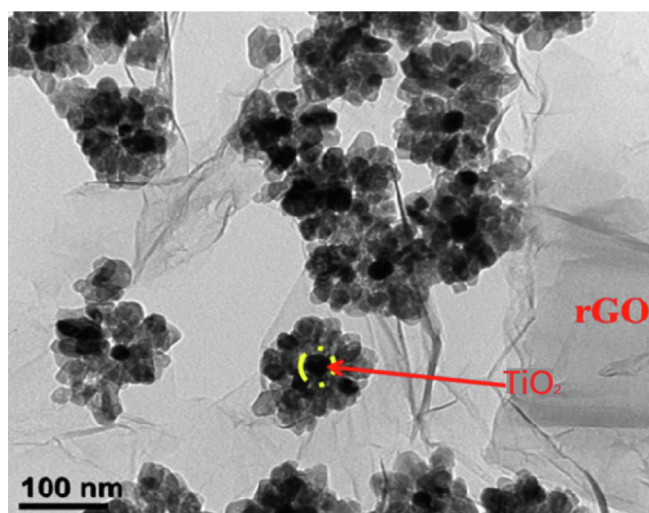
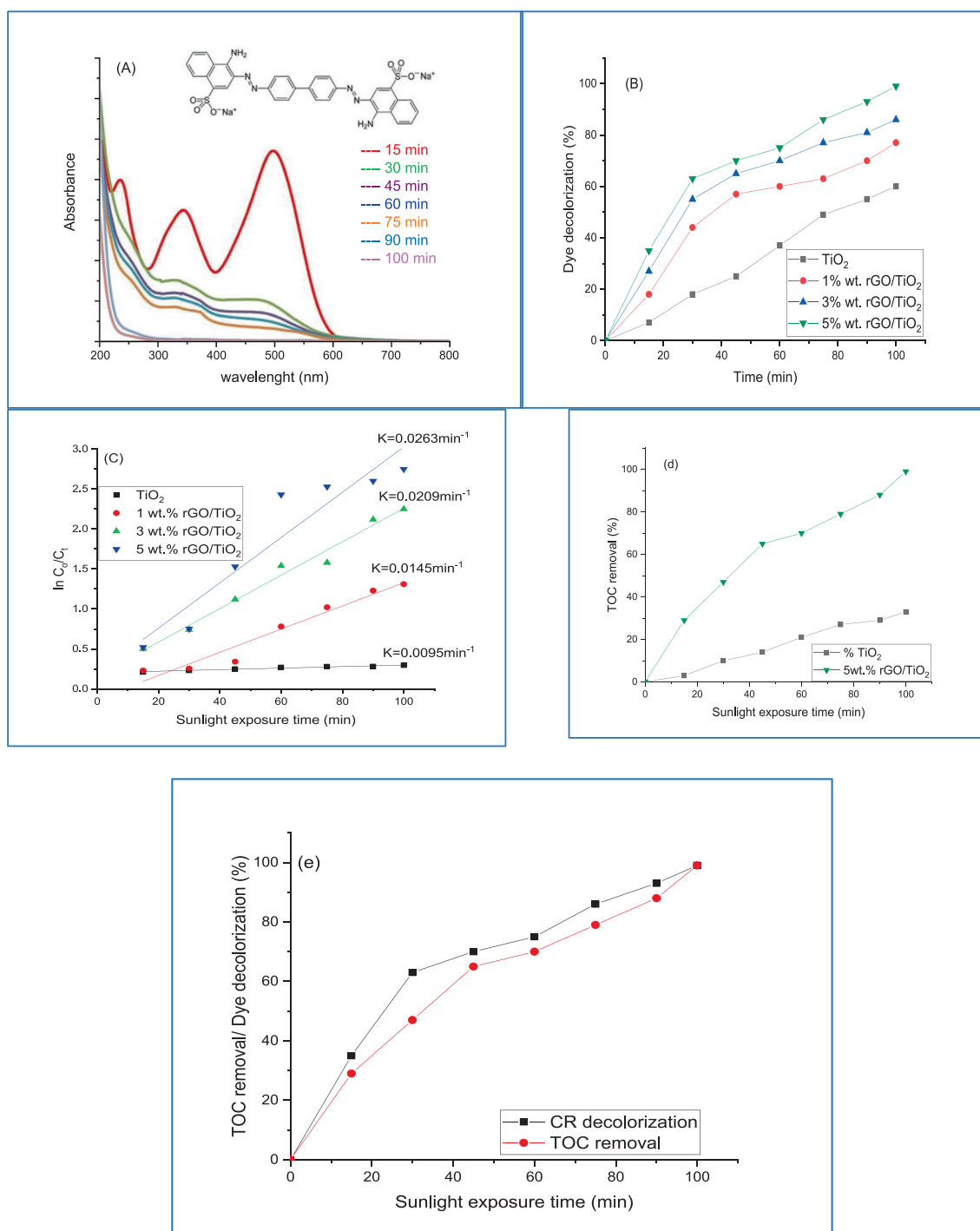


Fig. 6 TEM of 5 wt% rGO-TiO<sub>2</sub>.

500 nm, making a part of sunlight photons unattainable to the pure TiO<sub>2</sub> and 5 wt% rGO/TiO<sub>2</sub> catalysts. In Fig. 7b, the percentage decolorization of CR over pure TiO<sub>2</sub> and (1, 3 and 5) wt.% rGO/TiO<sub>2</sub> is shown. The findings indicate that the integration of TiO<sub>2</sub> is more effective in the degradation of dye when exposed to sunlight. Within the initial 15 min, the decolorization efficiency is 35% for 5 wt% rGO/TiO<sub>2</sub> in contrast to only 7% for the pure catalyst. The efficiency of degradation increases in proportion to the duration of sunlight exposure, ultimately reaching 99% after a time span of 100 min. The rate constant for the degradation of CR dye was calculated using Langmuir-Hinshelwood kinetic for pure TiO<sub>2</sub> and (1, 3 and 5)wt.% rGO/TiO<sub>2</sub> nanocomposites. The values of K are displayed in Fig. 7c. The findings demonstrate that the value of K for 5 wt% rGO/TiO<sub>2</sub> is greater than that of pure TiO<sub>2</sub>. This implies that the inclusion of rGO into the TiO<sub>2</sub> matrix results in a heightened efficiency of photo-excited electrons. Additionally, it leads to a reduction in charge carriers during the recombination process for pure TiO<sub>2</sub> (Movahedi et al., 2009). As the

studies mentioned (Ali et al., 2020); the CR dye undergoes a decolorization process rather than mineralization, as it loses its yellow color and forms intermediate compounds. This process occurs through an initial reaction with oxidizing agents such as hydroxyl free radicals and oxygen super anions, which also cause adsorption edge damage to the conjugation. To recognize between decolorization and mineralization, the Total Organic Carbon (TOC) measurements for 5 wt% rGO/TiO<sub>2</sub> and pure TiO<sub>2</sub> was carried out and the results are summarized in Fig. 7d. The findings demonstrate that the utilization of 5 wt % rGO/TiO<sub>2</sub> leads to a mineralization of the CR dye by a factor of 10. The comparison between decolorization and mineralization of CR dye under direct sunlight by using UV-Vis and TOC are shown in Fig. 7e. During the initial 15 min of exposure to sunlight, the decolorization of CR dye was observed to be 45%, while only 17% of organic matter was removed. This suggests that oxidative species are reacting with the dye to form intermediate compounds, resulting in fragmentation and damage to its conjugate structure, ultimately leading to



**Fig. 7** (A) CR decolorization UV-Vis spectrum at different time over 5 wt% rGO-TiO<sub>2</sub>, (B) comparison CR decolorization over pure and wt.% rGO-TiO<sub>2</sub>, (C) investigation plot of decolorization rate, (D) TOC removal of CR dye over pure and 5 wt% rGO-TiO<sub>2</sub>, (E) comparison of decolorization and mineralization of CR dye over 5 wt% rGO-TiO<sub>2</sub>.

its decolorization. The study showed that decreasing the concentration of CR led to an increase in the removal of organic carbon due to the oxidative species attack. It was noted earlier that TiO<sub>2</sub> has a favorable value for reducing oxygen, which is equal to  $-4.03$  V. This indicates that the formation of super oxygen anions is unavoidable (Ali et al., 2020).

### 3.3. LC-MS

The study investigated the liquid chromatography-mass spectroscopy analysis of photodegradation of CR dye under sunlight exposure for two different periods of time, namely 60 and 120 min, using 5%rGO/TiO<sub>2</sub> (Fig. 8a,b) depict LC-MS



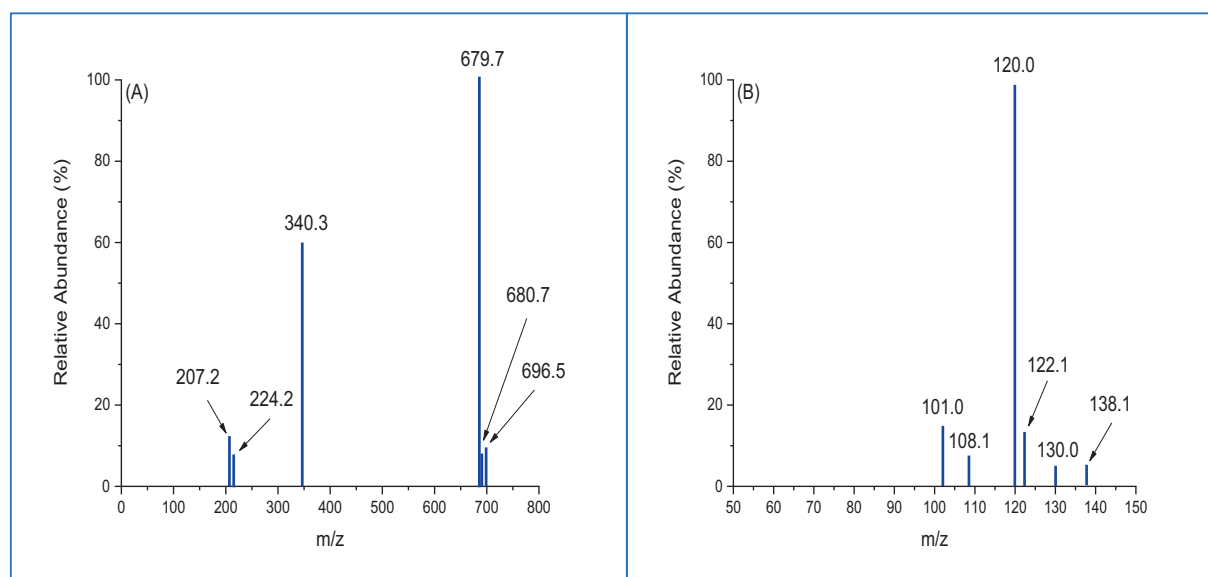


**Fig. 8** LC-MS of CR dye (A) before and (B) after decolorization.

spectra which exhibit distinct peaks at varying ( $m/z$ ) values that correspond to intermediate compounds, thus providing confirmation of the photodegradation of CR dye. The suggest pathway of CR dye photodegradation by using 5%rGO/TiO<sub>2</sub> is shown in Fig. 7. Firstly, the mechanism suggests that the cleaving of amine group and oxygenation of dye leads to the formation of a new compounds with  $m/z$  679 and 680 (Bhat et al., 2020) as shown in Fig. 8a. The results show two intensity peaks with  $m/z$  ratio of 244 and 207, which assign to hydrox-naphthalene -1-sulfonic acid result from cleavage of C<sub>6</sub>H<sub>6</sub> ring, N=N and C-N. Furthermore, the sustained activity of the OH free radical leads to the formation of 4-carboxybutanoate and naphthalene with respective molecular weights of 138 and 122 (Bhat et al., 2020). ROS, or reactive oxidative species, can cause the cleavage or reduction of sulfonic, amine nitro, and hydroxyl groups that are bonded with a C<sub>6</sub>H<sub>6</sub> ring. This process results in the production of 3-carboxyprppanoate, malonic acid, and malonate with  $m/z$  ratio of 120, 108 and 101 respectively (Shaban et al., 2017). The intermediate compounds of the thesis were effectively mineralized to CO<sub>2</sub> and H<sub>2</sub>O. The LC-MS findings indicated that complete degradation of CR under sunlight was achieved after 120 min using 5%rGO/TiO<sub>2</sub>. The proposed mechanism for CR decolorization is visually presented in Fig. 9.

### 3.4. The photocatalytic activity

The study examined the photocatalytic capabilities of synthesized compounds in the degradation of CR dye under direct sunlight. The photodegradation outcomes are presented in Fig. 10, which illustrates the decline of CR dye in pure and rGO-integrated TiO<sub>2</sub> nanocomposites with varying rGO concentrations (1%, 3%, and 5%). The concentration of CR dye prior to and after degradation under direct sunlight is represented by Co and Ci, respectively. The findings demonstrate that a mere 8% of CR dye underwent self-degradation when exposed to sunlight. However, the other photocatalysts that were prepared exhibited outstanding activity, with a 99% suc-

cess rate achieved by 5%rGO-TiO<sub>2</sub>. The results displayed in Fig. 10 demonstrate that samples incorporating rGO exhibit a greater capacity for CR dye compared to pure TiO<sub>2</sub>. This can be attributed to the increased surface area and  $\pi$ - $\pi$  system present in the rGO structure, which enhances the rate of reaction (Movahedi et al., 2009). The incorporation of rGO played a significant role in promoting the generation of hydroxyl free radicals, which ultimately results in the enhancement of congo red dye molecule breakdown through direct attack.

### 3.5. Electrochemical impedance (EIS) measurements

In order to predict the behavior of photo-excited carriers in the future, the electrochemical impedance spectrum (EIS) was utilized to study the transport and recombination characteristics of electron-hole carriers. The prepared samples were subjected to an applied bias of 0–0.5 V, and their Nyquist plot is depicted in Fig. 11. The typical plot demonstrating the photodegradation of congo red dye comprises two semicircles, which correspond to high and low frequency and represent charge transport resistance ( $R_{ct}$ ) and charge recombination process ( $R_{rec}$ ), respectively. The presence of two semicircles on the plot indicates that the degradation process involves the transfer or recombination of electrons-holes, which is an important step in determining the rate of degradation. The values of resistances ( $R_s$ ,  $R_{ct}$  and  $R_{rec}$ ) of prepared samples are summarized in Table. 2. The  $R_s$  values exhibit a decline as the rGO doping level rises. Conversely, the  $R_{rec}$  values experience an increase as the doping ratio increases, signifying the efficient separation of e-h with minimal recombination. The findings suggest that the sample doped with 5 wt% rGO exhibits activity in the photodegradation of CR dye, while also indicating that the easy inclusion of rGO can enhance carrier transportation. It is possible that the recombination process reduction can be attributed to two factors related to rGO. Firstly, the rGO may capture photoinduced excitons, which would lead to an increase in carrier concentration. Secondly, the rGO may serve to increase the surface area of TiO<sub>2</sub>, thus promoting rapid

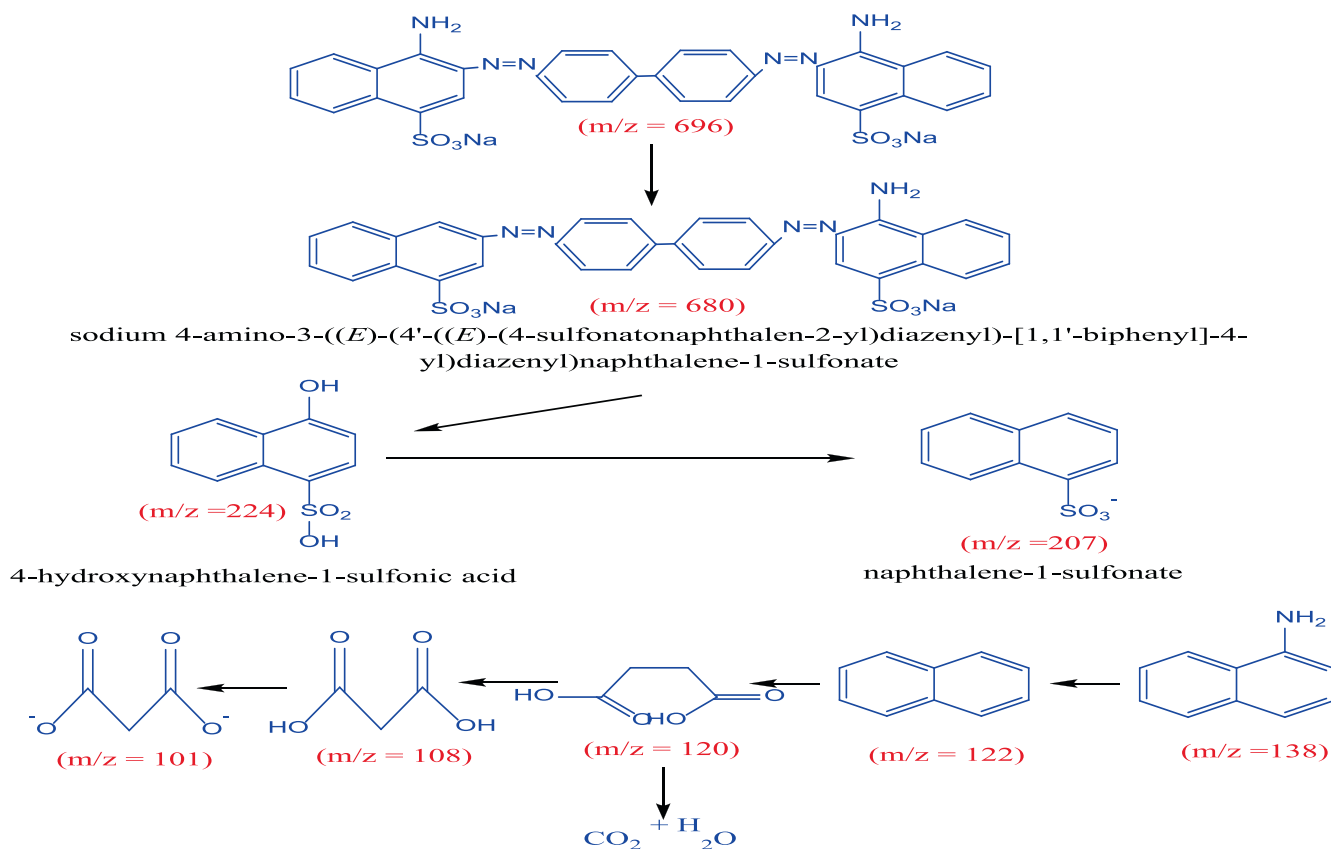


Fig. 9 Proposed decolorization path of CR dye.

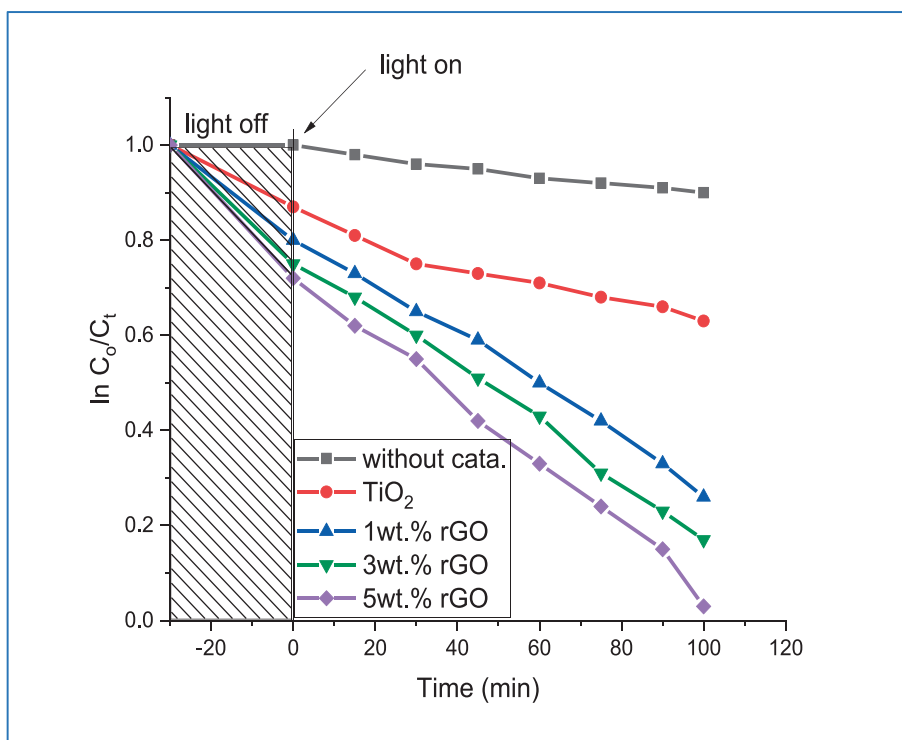
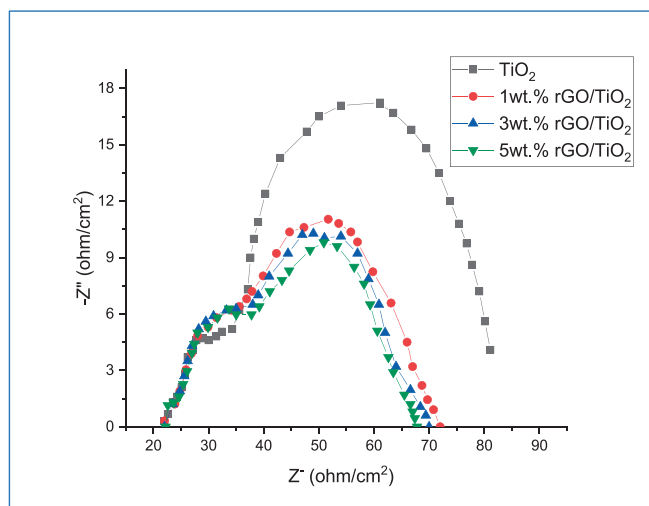


Fig. 10 Photodegradation of CR over catalyst.



**Fig. 11** EIS of pure and %rGO-TiO<sub>2</sub> under illumination conditions.

**Table 2** Electrochemical parameters of prepared compounds.

Sample	R <sub>s</sub>	R <sub>rec</sub>	R <sub>ct</sub>
TiO <sub>2</sub>	14	22	35
1 wt% rGO	15.10	82.45	21.56
3 wt% rGO	17.02	185.4	20.43
5 wt% rGO	12.56	300.23	18.06

transfer of photoinduced electrons to adsorbed oxygen on the surface of TiO<sub>2</sub> (Raya et al., 2022).

### 3.6. Charge electronic transference process and band diagram

In order to examine the electronic charge transfer process, we conducted PL spectrum and cyclic voltammetry (CV) analysis on both pure and 5 wt% rGO-TiO<sub>2</sub>. The PL spectrum of both prepared samples were showed and discussed in Fig. 4. The results demonstrate that both samples exhibit a similar spectrum, indicating comparable defects and electronic structure. The PL data confirms that the inclusion of TiO<sub>2</sub> in rGO effectively prevents charge recombination more than pure TiO<sub>2</sub>. However, the rate constant of standard heterogeneous, which determines the rate of electron transport in each material, was calculated using the Nicholson method (Martín-Yerga et al., 2016) and obtained through CV techniques under both dark and illuminated conditions. Fig. 12 presents the findings of an investigation on CVs utilizing thin-film electrodes composed of pure and 5 wt% rGO-TiO<sub>2</sub>. It seems that the cyclic voltogram for illumination did not exhibit frequent modulation with the dark voltogram for each of the electrodes that were prepared. The study found that compared to dark conditions, illuminating a pure TiO<sub>2</sub> electrode resulted in an increase in  $\Delta E$  of 0.460 V vs. SCE. In contrast, the 5 wt% rGO-TiO<sub>2</sub> electrode showed a decrease in  $\Delta E$  under illumination (0.468 V vs. SCE) compared to dark conditions (0.487 vs. SCE), as reported in Table 3. Under illumination conditions, the expansion of  $\Delta E$  values for both electrodes and a decrease

in the current of reduction and oxidation density are induced, as shown in Table 3. For the standard heterogeneous rate constant ( $k_0$ ) calculation, the coefficient of diffusion utilized were  $D_R = D_O = 0.726 * 10^{-5} \text{ cm}^2/\text{s}$  and the  $k_0$  values are displayed in Table 3 (Soares et al., 2016). The  $k_0$  values exhibited a degree of proximity, and the presence of a 5 wt% rGO-TiO<sub>2</sub> heterostructure resulted in decreased electron transfer. The process of illumination was observed to decrease electron transport in the electrode, indicating a possible increase in recombination. The 5 wt% rGO-TiO<sub>2</sub> heterostructure demonstrates that the absorbed light by doped rGO induces a noteworthy photothermal effect in the photocatalyst, thereby facilitating an increase in charge transfer (Low et al., 2017; Di et al., 2018; Merrad et al., 2023). The findings reveal that TiO<sub>2</sub> nanoparticles exhibit slightly higher  $k_0$  and recombination rates compared to the 5 wt% rGO-TiO<sub>2</sub> heterostructure. This suggests the importance of achieving a balance between recombination process and electron transport in the heterostructure sample, which ultimately enhances the photocatalytic efficiency.

### 3.7. Reusability of studies

To investigate the reusability of 5 wt% rGO-TiO<sub>2</sub> binary nanocomposite, a cycling experiment was carried out on CR dye up to four cycles and the results are shown in Fig. 13. After each cycle, 5 wt% rGO-TiO<sub>2</sub> was separated and washed to remove the CR dye and then dried at 80 °C for 10 h to utilize it for adsorption and photodegradation. The ratio of nanocomposite sample to dye concentration employed in the first cycle was maintained throughout subsequent cycles. The results indicate that the sample exhibits high capability with increasing cycle number, which suggests a high level of stability and potential suitability for the photodegradation of dyes.

### 3.8. Mechanism of CR photodegradation

Before proposing the mechanism of degradation, it is crucial to consider the scavenger effect in the study. This entails taking into account the presence of ROS, including hydroxyl free rad-

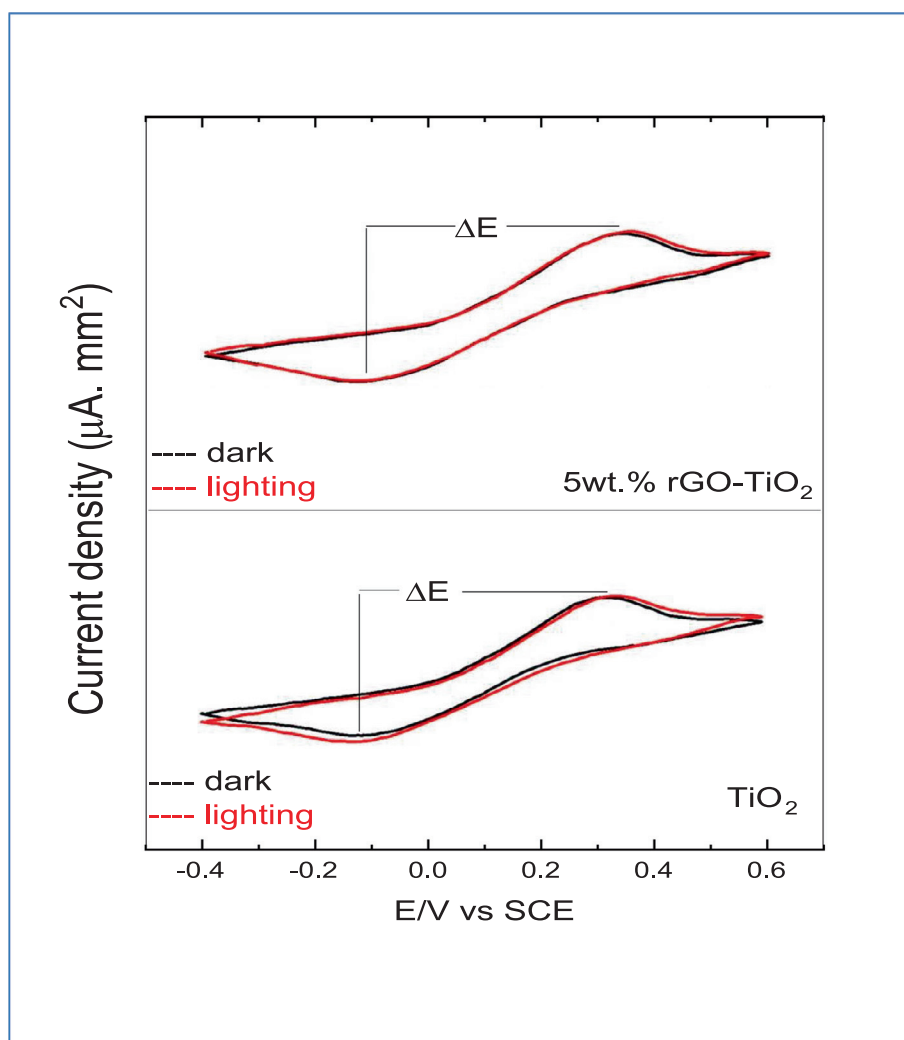


**Fig. 12** Cyclic Voltammograms of pure and 5 wt% rGO-TiO<sub>2</sub> electrodes in dark and lighting conditions.

**Table 3** Values of peak to peak separation ( $\Delta E$ ), the current density of oxidation and reduction calculated from cvs and  $K_o$  values.

Electrodes	$\Delta E$ (V vs. SCE)	$i_{\text{density oxidation}}$ ( $\mu\text{A}/\text{mm}^2$ )	$i_{\text{density reduction}}$ ( $\mu\text{A}/\text{mm}^2$ )	$K_o$ (cm/s)
TiO <sub>2</sub> – dark	0.425	2.70	-2.43	
TiO <sub>2</sub> – lighting	0.460	2.65	-2.55	-0.127
5 wt% rGO-TiO <sub>2</sub> – dark	0.468	2.75	-2.67	
5 wt% rGO-TiO <sub>2</sub> – lighting	0.487	2.60	-2.79	-0.133

icals, superoxide anions, as well as holes and electrons, which are all highly significant (Baruah et al., 2021). Four compounds of silver nitrate ( $e^-$ ), mannitol ( $\text{OH}^*$ ), benzoquinone ( $\text{h}^+$ ) and triethanolamine  $\text{O}_2^*$  were used as a scavenger for examining the effect of radical (Fig. 14) on the photodegradation of CR under sunlight. The findings indicate that scavenger compounds significantly reduce photodegradation efficiency by more than 50%. However, the use of  $\text{AgNO}_3$  does not appear to have an effect on the photodegradation mechanism. The application of benzoquinone as a scavenger is substantiated by its crucial role in the mechanism pathway (Ali et al.,

2022), which signifies its primary involvement in the generation of  $\text{OH}^*$  from water and consequent degradation of CR dye. The addition of benzoquinone to the reaction system resulted in the inhibition of CR degradation.

The integration of rGO with TiO<sub>2</sub> is considered a viable option for facilitating the transfer and acceptance of excited electrons from the TiO<sub>2</sub> CB. This is primarily due to the planar structure, as depicted in Fig. 15. The rapid separation of carriers, achieved through the incorporation of a substance, has been observed to contribute to the restraint of electron-hole recombination process and achieve high rates. Additionally,

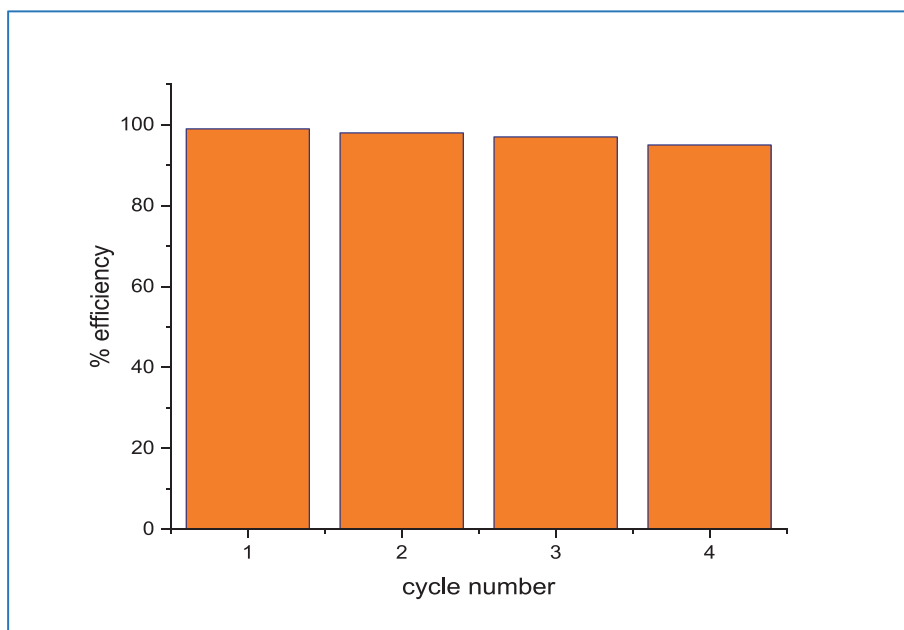


Fig. 13 The reusability of 5wt.%rGO-TiO<sub>2</sub> for up to four cycles.

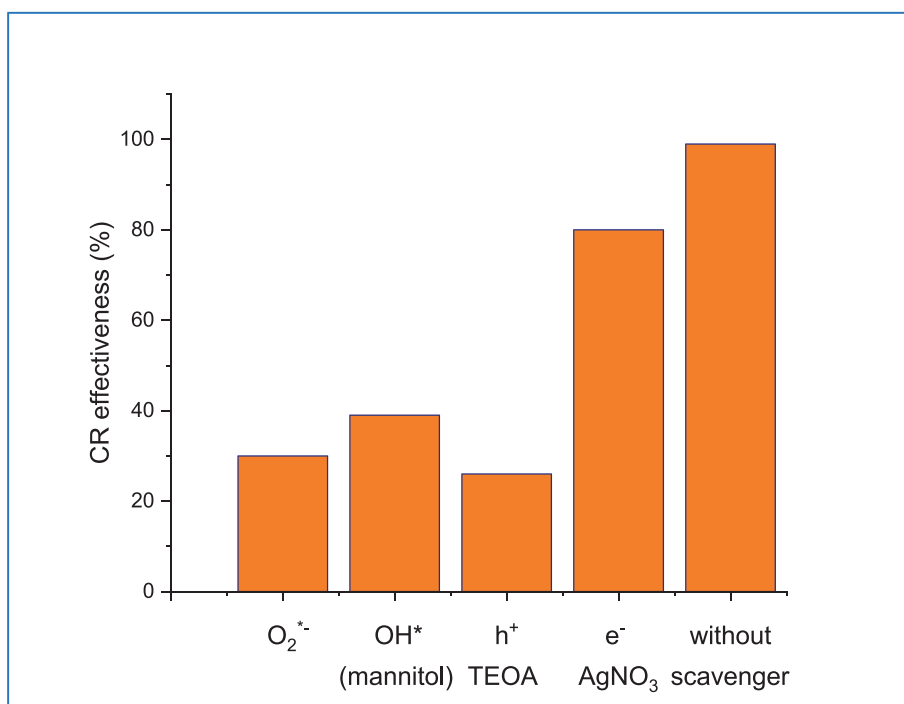


Fig. 14 photodegradation of CR under different scavenger.

this incorporation has been shown to improve the visible light adsorption of TiO<sub>2</sub> and expand it in comparison with pure TiO<sub>2</sub>. The rGO/TiO<sub>2</sub> photo catalyst exhibits a high level of efficiency in the adsorption of the CR dye due to its planar structure, which facilitates a platform for the dye to be adsorbed.

### 3.9. Computational details

Theoretical analysis was conducted on various pH levels using the Gaussian 09 W software. The optimization of geometry and reactivity of congo red dye towards catalyst were investigated and carried out via density function theory (DFT) with



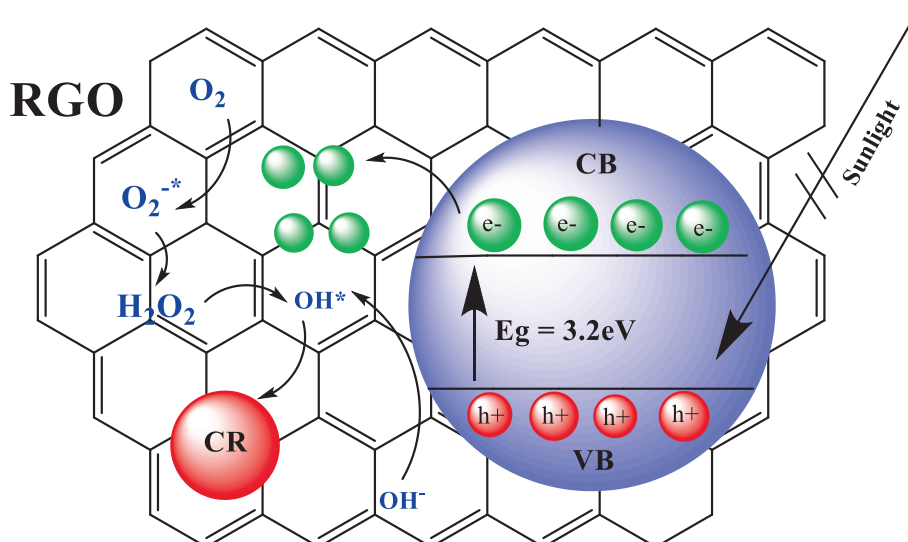


Fig. 15 Proposed mechanism CR photodegradation at optimum condition over 5 wt% rGO-TiO<sub>2</sub>.

Backers parameter of exchange functional (Ali et al., 2022). Additionally, a split-valence double zeta basis set 6.31G(d) and Lee-Yang-Parr (B3LYP) correlation function was employed in the calculation (Becke, 1993). Upon optimization, several theoretical properties were examined, including HOMO, LUMO, ionization energy, electron affinity, softness and hardness. The DFT calculations indicate a relationship and interaction between the 5wt.%rGO-TiO<sub>2</sub> catalyst and both anionic and cationic congo red dyes (Koch and Holthausen, 2015). Theoretical reactivity parameters such as E HOMO, E LUMO, softness, hardness, electrophilicity and electronic chemical potential were determined using a reaction catalyst and Congo Red dye species (CR=N=NH, CR=N-NH and CR=N=N). The obtained results are presented in Fig. 16 and Table. 4.

The chemical hardness, softness and electronic chemical potential calculated from the following equations (Domingo et al., 2016; Parr and Yang, 1984):

$$h = -0.5(E_{\text{HOMO}} - E_{\text{LUMO}}) \quad (2)$$

$$m = 0.5(E_{\text{HOMO}} + E_{\text{LUMO}}) \quad (3)$$

$$\bar{\omega} = \mu/2\eta \quad (4)$$

Generally, The exchange capacity of electron density among congo red species dye is contingent upon the potential of chemical electronic ( $\mu$ ) (Parr et al., 1999). When the molecules exhibit high values of  $\mu$ , it indicates the presence of potent electron-acceptor molecules. Conversely, a low value of  $\eta$  signifies increased reactivity (Bredas, 2014). The high

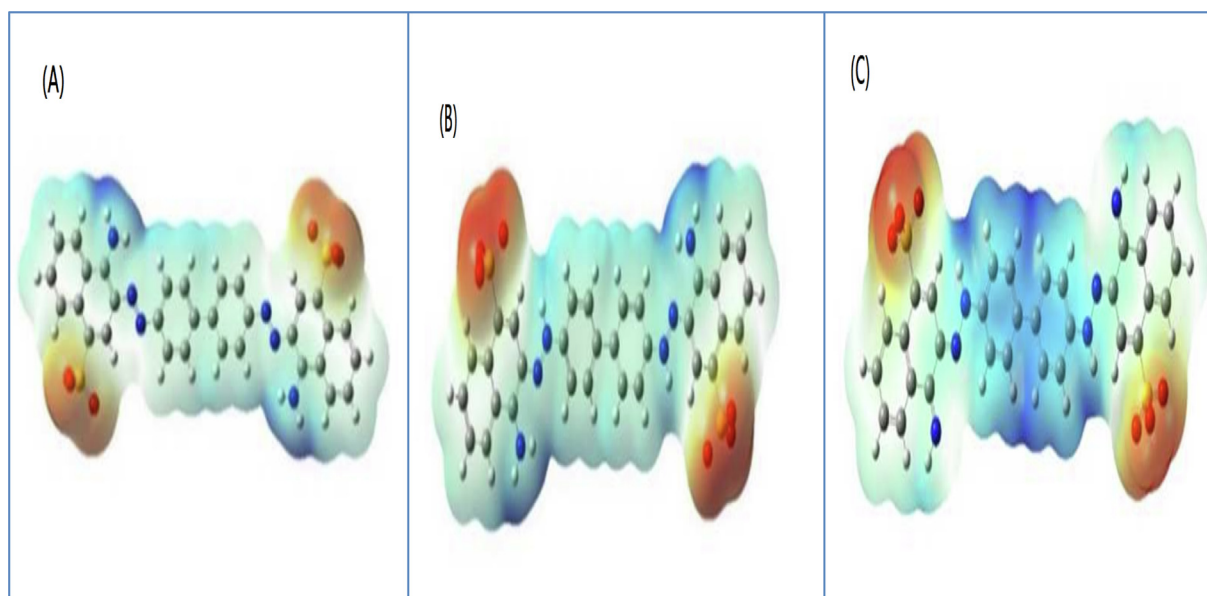


Fig. 16 Electron density mapping of (A) CR-N = N, (B) CR-N = NH and (C) CR = N-NH.

**Table 4** HOMO, LUMO, hardness and softness of congo red species.

Dye species	E(eV) HOMO	E(eV) LUMO	E <sub>g</sub> (eV)	η	S softness	μ	$\bar{\omega}$
CR-N = N	-6.1	-5.7	-0.4	3.25	0.31	-5.9	5.36
CR-N = NH	-5.4	-4.2	-1.2	3.30	0.30	-4.8	3.49
CR = N-NH	-8.9	-5.4	-3.5	6.22	0.16	-7.15	4.11

value of  $\bar{\omega}$ , has an inverse effect on the ability of dye species to accept electron load. According to the data presented in Table 3, the smallest value of parameter  $\eta$  is associated with CR-N=N species, which makes it more likely to interact with 5wt.%rGO-TiO<sub>2</sub> compared to other species. Furthermore, this species has the smallest energy gap when compared to other species, which accelerates photodegradation by promoting recombination of hole-electron pairs (Valadi et al., 2020). At low pH, the CR-N=NH species exhibits electrophilicity of 3.49, which is lower than that of CR-N=N and CR=N-NH, which have electrophilicities of 5.36 and 4.11, respectively. This makes it easier for the CRN=NH species to be oxidized by OH free radicals and O super anions. Additionally, in an acidic medium, TiO<sub>2</sub> forms TiOH<sub>2</sub> which can adsorb more anionic species of CR-N=NH and CR=N-NH, thus improving its degrading capabilities (Thomas et al., 2016; Soares et al., 2021).

#### 4. Conclusion

To summarize, the incorporation of TiO<sub>2</sub> in rGO led to an improvement in light absorption within the visible region. Additionally, this process effectively eliminated undesired electron-hole pairs through enhanced transfer of photogenerated electrons to reductants. It was also observed that superoxide anion radicals played a crucial role in the photocatalytic mineralization and decolorization. A series of TiO<sub>2</sub> binary nanocomposites with varying weight ratios of rGO were produced using the photolysis-humer modified method. The photocatalytic performance of each composite was assessed for its ability to remove congo red dye (CR) when exposed to direct sunlight. The incorporation of rGO in anatase TiO<sub>2</sub> surface was characterized by XPS, Raman and XRD. The UV-Vis spectrum of rGO-TiO<sub>2</sub> nanocomposite exhibited a red shift and a reduction in band gap energy compared to pure TiO<sub>2</sub>. The XRD analysis revealed that the decrease in rGO ratio corresponded with a reduction in crystalline size. The doping process caused a change in lattice parameters, indicating that rGO may have entered the crystal lattice of TiO<sub>2</sub>. The TEM analysis reveals that the rGO sheets contain TiO<sub>2</sub> particles with a size of approximately 10 nm and are evenly dispersed. The nanocomposite with a 5 wt% concentration of rGO-TiO<sub>2</sub> exhibited the least intense photoluminescence and the highest level of activity due to a reduction in electron-hole recombination, a decrease in R<sub>ct</sub>, and an increase in the production of potential oxidizing species. The improved photocatalytic effectiveness of rGO-doped TiO<sub>2</sub> with respect to pure TiO<sub>2</sub> results from various factors. (i), the morphology exhibits well-dispersed anatase TiO<sub>2</sub> nanoparticles throughout rGO sheets. (ii), the reduction characteristics of rGO play a role. (iii), there is a sharp increase in visible light absorption. (iv), there is a

decrease in the band gap. (v), faster electron transport and reduced recombination of charge carriers contribute to the enhanced efficiency. Recycling experiments demonstrate high stability and integrity of 5 wt% rGO-TiO<sub>2</sub>.

#### 5. Author statement

We know of no conflict of interest associated with this publication, and there has been no financial support for this work that could have influenced its outcome as corresponding author, I confirm that the manuscript has been read and approved for submission by all the named authors.

#### Data availability

All data generated or analyzed during this study are included in this published article.

#### Declaration of Competing Interest

We wish to confirm that there are no known conflicts of interest associated with this publication and there has been no significant financial support for this work that could have influenced its outcome.

#### Appendix A. Supplementary material

Supplementary data to this article can be found online at <https://doi.org/10.1016/j.arabjc.2023.104992>.

#### References

- Ali, M.H.H., Goher, M.E., Al-Afify, A.D.G., et al, 2022. A facile method for synthesis rGO/Ag nanocomposite and its uses for enhancing photocatalytic degradation of Congo red dye. *SN Appl. Sci.* 4, 276. <https://doi.org/10.1007/s42452-022-05163-0>.
- Ali, N., Said, A., Ali, F., et al, 2020. Photocatalytic degradation of congo red dye from aqueous environment using cobalt ferrite nanostructures: development, characterization, and photocatalytic performance. *Water Air Soil Pollut.* 231, 50. <https://doi.org/10.1007/s11270-020-4410-8>.
- Al-Kandari, S., Abdullah, A.M., Al-Kandari, H., et al, 2021. Eco-friendly highly efficient BN/rGO/TiO<sub>2</sub> nanocomposite visible-light photocatalyst for phenol mineralization. *Environ. Sci. Pollut Res.* 28, 62771–62781. <https://doi.org/10.1007/s11356-021-15083-y>.
- Al-Obaidi, N.S., Sadeq, Z.E., Mahmoud, Z.H., Abd, A.N., Al-Mahdawi, A.S., Ali, F.K., 2023. Synthesis of Chitosan-TiO<sub>2</sub> Nanocomposite for Efficient Cr (VI) Removal from Contaminated Wastewater Sorption Kinetics, Thermodynamics and Mechanism. *Journal of Oleo. Science* 72 (3).
- Andreozzi, M., Álvarez, M.G., Contreras, S., et al, 2018. Treatment of saline produced water through photocatalysis using rGO-TiO<sub>2</sub>

- nanocomposites. *Catal. Today.* <https://doi.org/10.1016/j.cattod.2018.04.048>.
- Ansari, A.R., Ansari, S.A., Parveen, N., et al, 2022. Silver nanoparticles decorated on the surface of reduced graphene oxide coated titanium oxide nanocomposite for enhanced electrochemical supercapacitance performance. *Ionics* 28, 4793–4804. <https://doi.org/10.1007/s11581-022-04685-2>.
- Aoudjit, L., Zioui, D., Touahra, F., et al, 2021. Photocatalytic degradation of tartrazine dyes using TiO<sub>2</sub>-Chitosan beads under sun light irradiation. *Russ. J. Phys. Chem.* 95, 1069–1076. <https://doi.org/10.1134/S0036024421050034>.
- Baruah, M., Ezung, S.L., Supong, A., et al, 2021. Synthesis, characterization of novel Fe-doped TiO<sub>2</sub> activated carbon nanocomposite towards photocatalytic degradation of Congo red, E. coli, and S. aureus. *Korean J. Chem. Eng.* 38, 1277–1290. <https://doi.org/10.1007/s11814-021-0830-4>.
- Becke, A.D., 1993. A new mixing of Hartree-Fock and local density-functional theories. *J. Chem. Phys.* 98, 1372–1377.
- Bhat, S.A., Zafar, F., Mondal, A.H., et al, 2020. Photocatalytic degradation of carcinogenic Congo red dye in aqueous solution, antioxidant activity and bactericidal effect of NiO nanoparticles. *J. Iran Chem. Soc.* 17, 215–227. <https://doi.org/10.1007/s13738-019-01767-3>.
- Bredas, J.-L., 2014. Mind the gap! *Mater. Horiz.* 1, 17–19.
- Chen, Y., Dong, X., Cao, Y., et al, 2017. Enhanced photocatalytic activities of low-bandgap TiO<sub>2</sub>-reduced graphene oxide nanocomposites. *J. Nanopart Res* 19, 200. <https://doi.org/10.1007/s11051-017-3871-1>.
- Chen, F., Feng, H.F., Luo, W., et al, 2021. Simultaneous realization of direct photodeposition and high H<sub>2</sub>-production activity of amorphous cobalt sulfide nanodot-modified rGO/TiO<sub>2</sub> photocatalyst. *Rare Met.* 40, 3125–3134. <https://doi.org/10.1007/s12598-021-01755-8>.
- Chetibi, L., Busko, T., Kulish, N.P., et al, 2017. Photoluminescence properties of TiO<sub>2</sub> nanofibers. *J. Nanopart Res* 19, 129. <https://doi.org/10.1007/s11051-017-3822-x>.
- Di, L., Yang, H., Xian, T., et al, 2018. Facile synthesis and enhanced visible-light photocatalytic activity of novel p-Ag<sub>3</sub>PO<sub>4</sub>/n-BiFeO<sub>3</sub> heterojunction composites for dye degradation. *Nanoscale Res Lett* 13, 257. <https://doi.org/10.1186/s11671-018-2671-6>.
- Domingo, L.R., Ríos-Gutiérrez, M., Pérez, P., 2016. Applications of the conceptual density functional theory indices to organic chemistry reactivity. *Molecules* 21, 748.
- Dong, K., He, J., Liu, J., et al, 2017. Photocatalytic performance of Cu<sub>2</sub>O-loaded TiO<sub>2</sub>/rGO nanoheterojunctions obtained by UV reduction. *J. Mater Sci* 52, 6754–6766. <https://doi.org/10.1007/s10853-017-0911-2>.
- Du, C., Liu, G., Qu, Z., et al, 2022. GO/TiO<sub>2</sub>-decorated electrospun polyvinylidene fluoride membrane prepared based on metal-polyphenol coordination network for oil-water separation and desalination. *J. Mater. Sci.* 57, 3452–3467. <https://doi.org/10.1007/s10853-021-06824-y>.
- Fang, R., Liang, Y., Ge, X., et al, 2015. Preparation and photocatalytic degradation activity of TiO<sub>2</sub>/rGO/polymer composites. *Colloid Polym. Sci.* 293, 1151–1157. <https://doi.org/10.1007/s00396-015-3507-x>.
- Farhan, M.A., Mahmoud, Z.H., Falih, M.S., 2018. Synthesis and characterization of TiO<sub>2</sub>/Au nanocomposite using UV-Irradiation method and its photocatalytic activity to degradation of methylene blue. *Asian J. Chem* 30.
- Fathy, M., Gomaa, A., Taher, F.A., et al, 2016. Optimizing the preparation parameters of GO and rGO for large-scale production. *J. Mater. Sci.* 51, 5664–5675. <https://doi.org/10.1007/s10853-016-9869-8>.
- Holzwarth, U., Gibson, N., 2011. The Scherrer equation versus the 'Debye-Scherrer equation'. *Nature Nanotech.* 6, 534. <https://doi.org/10.1038/nnano.2011.145>.
- John, D., Rajalakshmi, A.S., Lopez, R.M., et al, 2020. TiO<sub>2</sub>-reduced graphene oxide nanocomposites for the trace removal of diclofenac. *SN Appl. Sci.* 2, 840. <https://doi.org/10.1007/s42452-020-2662-y>.
- Karthik, P., Gowthaman, P., Venkatachalam, M., et al, 2020. Propose of high performance resistive type H<sub>2</sub>S and CO<sub>2</sub> gas sensing response of reduced graphene oxide/titanium oxide (rGO/TiO<sub>2</sub>) hybrid sensors. *J. Mater. Sci: Mater. Electron* 31, 3695–3705. <https://doi.org/10.1007/s10854-020-02928-4>.
- Khatmi Maab, N.Z., Shokuhfar, A., Ahmadi, S., 2016. The effect of temperature and type of peroxide on graphene synthesized by improved Hummers' method. *Int. Nano Lett.* 6, 211–214. <https://doi.org/10.1007/s40089-016-0179-6>.
- Koch, W., Holthausen, M.C., 2015. *A Chemist's Guide to Density Functional Theory.* John Wiley & Sons., Hoboken, NJ, USA.
- Krishnamoorthy, K., Veerapandian, M., Mohan, R., et al, 2012. Investigation of Raman and photoluminescence studies of reduced graphene oxide sheets. *Appl. Phys. A* 106, 501–506. <https://doi.org/10.1007/s00339-011-6720-6>.
- Kundu, A., Mondal, A., 2019. Photodegradation of methylene blue under direct sunbeams by synthesized anatase titania nanoparticles. *SN Appl. Sci.* 1, 280. <https://doi.org/10.1007/s42452-019-0280-3>.
- Liu, Y., Zhou, Y., Yang, L., et al, 2016. Hydrothermal synthesis of 3D urchin-like Ag/TiO<sub>2</sub>/reduced graphene oxide composites and its enhanced photocatalytic performance. *J. Nanopart Res* 18, 283. <https://doi.org/10.1007/s11051-016-3596-6>.
- Long, Y., Qin, C.C., et al, 2013. Origin of visible light photoactivity of reduced graphene oxide/TiO<sub>2</sub> by in situ hydrothermal growth of undergrown TiO<sub>2</sub> with Graphene Oxide. *J. Phys. Chem. C* 117, 16734–16741.
- Low, J., Yu, J., Jaroniec, M., et al, 2017. Heterojunction photocatalysts. *Adv. Mater.* <https://doi.org/10.1002/adma.201601694>.
- Ma, Y., Wang, S., Zheng, W., et al, 2021. Preparation of N-TiO<sub>2</sub>/RGO nanocomposites through sol-gel method. *Korean J. Chem. Eng.* 38, 1913–1922. <https://doi.org/10.1007/s11814-021-0843-z>.
- Mahmoud, Z.H., Falih, M.S., Khalaf, O.E., Farhan, M.A., Ali, F.K., 2018. Photosynthesis of AgBr doping TiO<sub>2</sub> nanoparticles and degradation of reactive red 120 dye. *J. Adv. Pharm. Education Res.* 8.
- Mahmoud, Z.H., Al-Bayati, R.A., Khadom, A.A., 2021. Enhanced photovoltaic performance of dye-sanitized solar cell with tin doped titanium dioxide as photoanode materials. *Chalcogenide Lett.* 18 (12).
- Mahmoud, Z.H., Al-Bayati, R.A., Khadom, A.A., 2022. Synthesis and supercapacitor performance of polyaniline-titanium dioxide-samarium oxide (PANI/TiO<sub>2</sub>-Sm<sub>2</sub>O<sub>3</sub>) nanocomposite. *Chem. Pap.* 76, 1401–1412. <https://doi.org/10.1007/s11696-021-01948-6>.
- Mahmoud, Z.H., Al-Bayati, R.A., Khadom, A.A., 2022. The efficacy of samarium loaded titanium dioxide (Sm: TiO<sub>2</sub>) for enhanced photocatalytic removal of rhodamine B dye in natural sunlight exposure. *J. Mol. Struct.* 1253.
- Mahmoud, Z.H., Al-Bayati, R.A., Khadom, A.A., 2022. Electron transport in dye-sanitized solar cell with tin-doped titanium dioxide as photoanode materials. *J. Mater. Sci.: Mater. Electron.* 33.
- Mahmoud, Z.H., Hammoudi, O.G., Abd, A.N., Ahmed, Y.M., Altamari, U.S., Dawood, A.H., Shaker, R., 2023. Functionalize cobalt ferrite and ferric oxide by nitrogen organic compound with high supercapacitor performance. *Results Chem.* 5. <https://doi.org/10.1016/j.rechem.2023.100936>.
- Martin-Yerga, D., Rama, E.C., Costa-García, A., 2016. Electrochemical characterization of ordered mesoporous carbon screen-printed electrodes. *J. Electrochem. Soc.* 163, B176–B179. <https://doi.org/10.1149/2.0871605jes>.
- Merrad, S., Abbas, M., Brahimi, R., et al, 2023. Physical properties of the perovskite SrTiO<sub>3</sub>-δ synthesized by chemical route. *J. Mater. Sci.: Mater. Electron* 34, 206. <https://doi.org/10.1007/s10854-022-09616-5>.

- Moushumi, Z.M., Hassan, M.J., Ahsan, M., et al, 2022. Photocatalytic degradation of chlorazol yellow dye under sunlight irradiation using Ce, Bi, and N co-doped TiO<sub>2</sub> photocatalyst in neutral medium. *Environ. Sci. Pollut. Res.* <https://doi.org/10.1007/s11356-022-24220-0>.
- Moustafa, H.M., Mahmoud, M.S., Nassar, M.M., 2022. Kinetic analysis of p-rGO/n-TiO<sub>2</sub> nanocomposite generated by hydrothermal technique for simultaneous photocatalytic water splitting and degradation of methylene blue dye. *Environ. Sci. Pollut. Res.* <https://doi.org/10.1007/s11356-022-23430-w>.
- Movahedi, M., Mahjoub, A.R., Janitabar-Darzi, S., 2009. Photodegradation of Congo red in aqueous solution on ZnO as an alternative catalyst to TiO<sub>2</sub>. *JICS* 6, 570–577. <https://doi.org/10.1007/BF03246536>.
- Nasralla, N.H.S., Yeganeh, M., Šiller, L., 2020. Photoluminescence study of anatase and rutile structures of Fe-doped TiO<sub>2</sub> nanoparticles at different dopant concentrations. *Appl. Phys. A* 126, 192. <https://doi.org/10.1007/s00339-020-3379-x>.
- Parr, R.G., Yang, W., 1984. Density functional approach to the frontier-electron theory of chemical reactivity. *J. Am. Chem. Soc.* 106, 4049–4050.
- Parr, R.G., Szentpály, L.V., Liu, S., 1999. Electrophilicity index. *J. Am. Chem. Soc.* 121, 1922–1924.
- Raya, I., Kzar, H.H., Mahmoud, Z.H., et al, 2022. A review of gas sensors based on carbon nanomaterial. *Carbon Lett.* 32, 339–364. <https://doi.org/10.1007/s42823-021-00276-9>.
- Reza, K.M., Kurny, A., Gulshan, F., 2017. Parameters affecting the photocatalytic degradation of dyes using TiO<sub>2</sub>: a review. *Appl. Water Sci.* 7, 1569–1578. <https://doi.org/10.1007/s13201-015-0367-y>.
- Saeed, K., Khan, I., Gul, T., et al, 2017. Efficient photodegradation of methyl violet dye using TiO<sub>2</sub>/Pt and TiO<sub>2</sub>/Pd photocatalysts. *Appl. Water Sci.* 7, 3841–3848. <https://doi.org/10.1007/s13201-017-0535-3>.
- Saher, R., Hanif, M.A., Mansha, A., et al, 2021. Sunlight-driven photocatalytic degradation of rhodamine B dye by Ag/FeWO<sub>4</sub>/g-C<sub>3</sub>N<sub>4</sub> composites. *Int. J. Environ. Sci. Technol.* 18, 927–938. <https://doi.org/10.1007/s13762-020-02888-6>.
- Sang, L., Lei, L., Burda, C., 2019. Electrochemical Fabrication of rGO-embedded Ag-TiO<sub>2</sub> Nanoring/Nanotube Arrays for Plasmonic Solar Water Splitting. *Nano-Micro Lett.* 11, 97. <https://doi.org/10.1007/s40820-019-0329-2>.
- Shaban, M., Abukhadra, M.R., Ibrahim, S.S., et al, 2017. Photocatalytic degradation and photo-Fenton oxidation of Congo red dye pollutants in water using natural chromite—response surface optimization. *Appl. Water Sci.* 7, 4743–4756. <https://doi.org/10.1007/s13201-017-0637-y>.
- Shen, J., Shi, M., Yan, B., et al, 2011. Ionic liquid-assisted one-step hydrothermal synthesis of TiO<sub>2</sub>-reduced graphene oxide composites. *Nano Res.* 4, 795–806. <https://doi.org/10.1007/s12274-011-0136-7>.
- Singh, N., Jana, S., Singh, G.P., et al, 2022. Plasmonic Au-rGO-TiO<sub>2</sub> ternary photocatalyst for photocatalytic hydrogen production and dye degradation. *Nanotechnol. Environ. Eng.* 7, 119–137. <https://doi.org/10.1007/s41204-021-00199-w>.
- Soares, L.G., de Oliveira Vaz, M., Teixeira, S.R., Alves, A.K., 2021. Absorbance determination and photocatalytic production of hydrogen using tungsten and TiO<sub>2</sub> oxide nanostructures As catalyst. *Clean. Eng. Technol.* 5, 100268.
- Soares, G.B., Ribeiro, R.A.P., De Lazaro, S.R., Ribeiro, C., 2016. Photoelectrochemical and theoretical investigation of the photocatalytic activity of TiO<sub>2</sub>: N. *RSC Adv.* <https://doi.org/10.1039/c6ra15825k>.
- Thomas, M., Naikoo, G.A., Sheikh, M.U.D., Bano, M., Khan, F., 2016. Effective photocatalytic degradation of Congo red dye using alginate/carboxymethyl cellulose/TiO<sub>2</sub> nanocomposite hydrogel under direct sunlight irradiation. *J. Photochem. Photobiol. A: Chem.* 327, 33–43.
- Valadi, F.M., Ekramipooya, A., Gholami, M.R., 2020. Selective separation of Congo Red from a mixture of anionic and cationic dyes using magnetic-MOF: experimental and DFT study. *J. Mol. Liq.* 318, 114051.
- Wang, N., Zhang, F., Mei, Q., et al, 2020. Photocatalytic TiO<sub>2</sub>/rGO/CuO Composite for Wastewater Treatment of Cr(VI) Under Visible Light. *Water Air Soil Pollut* 231, 223. <https://doi.org/10.1007/s11270-020-04609-8>.
- Yue, H.Y., Guan, E.H., Gao, X., et al, 2019. One-step hydrothermal synthesis of TiO<sub>2</sub> nanowires-reduced graphene oxide nanocomposite for supercapacitor. *Ionics* 25, 2411–2418. <https://doi.org/10.1007/s11581-018-2678-0>.